EC
26,8

Received 14 April 2008
Revised 17 September 2008
Accepted 13 March 2009

Boundary element analysis of mixed-mode stress intensity factors in an anisotropic cuboid with an inclined surface crack

Chia-Hau Chen and Chao-Shi Chen
Department of Resources Engineering, National Cheng Kung University, Tainan, Taiwan
Ernian Pan
Department of Civil Engineering, University of Akron, Akron, Ohio, USA
Han-Chou Tseng
Department of Resources Engineering, National Cheng Kung University, Tainan, Taiwan, and
Pao-Shan Yu
Department of Hydraulic and Ocean Engineering, National Cheng Kung University, Tainan, Taiwan

Abstract

Purpose – The purpose of this paper is to present special nine-node quadrilateral elements to discretize the un-cracked boundary and the inclined surface crack in a transversely isotropic cuboid under a uniform vertical traction along its top and bottom surfaces by a three-dimensional (3D) boundary element method (BEM) formulation. The mixed-mode stress intensity factors (SIFs), K_I, K_{II} and K_{III}, are calculated.

Design/methodology/approach – A 3D dual-BEM or single-domain BEM is employed to solve the fracture problems in a linear anisotropic elastic cuboid. The transversely isotropic plane has an arbitrary orientation, and the crack surface is along an inclined plane. The mixed 3D SIFs are evaluated by using the asymptotical relation between the SIFs and the relative crack opening displacements.

Findings – Numerical results show clearly the influence of the material and crack orientations on the mixed-mode SIFs. For comparison, the mode-I SIF when a horizontal rectangular crack is embedded entirely within the cuboid is calculated also. It is observed that the SIF values along the crack front are larger when the crack is closer to the surface of the cuboid than those when the crack is far away from the surface.

Research limitations/implications – The FORTRAN program developed is limited to regular surface cracks which can be discretized by the quadrilateral shape function; it is not very efficient and suitable for irregular crack shapes.

Practical implications – The evaluation of the 3D mixed-mode SIFs in the transversely isotropic material may have direct practical applications. The SIFs have been used in engineering design to obtain the safety factor of the elastic structures.

Originality/value – This is the first time that the special nine-node quadrilateral shape function has been applied to the boundary containing the crack mouth. The numerical method developed can be applied to the SIF calculation in a finite transversely isotropic cuboid within an inclined surface crack. The computational approach and the results of SIFs are of great value for the modeling and design of anisotropic elastic structures.

Keywords Surface properties of materials, Stress (materials), Physical properties of materials, Elastic analysis

Paper type Research paper

The project is sponsored by NCKU under grant number R046. The authors thank the reviewers and Editor for their beneficial comments and suggestions.

Engineering Computations: International Journal for Computer-Aided Engineering and Software
Vol. 26 No. 8, 2009
pp. 1056-1073

0264-4401
DOI 10.1108/02644400910996899

1. Introduction

Defects are commonly originated from the free surface. They are inherent to the structural materials or are developed during manufacturing and fabrication. Thus, study of surface cracks is fundamental to fracture analysis of the involved structure. Regardless of how a surface crack is initiated or introduced in a component, accurate prediction of the fracture conditions (i.e. mixed-mode stress intensity factors (SIFs)) is very important in solid mechanics. There are three basic modes of crack tip deformation in the fracture process: mode-I (tension, opening), mode-II (in-plane shear, sliding) and mode-III (out-of-plane shear, tearing). The fracture mechanical safety of a solid elastic structure can be designed depended on these SIFs (Toribio and Kharin, 1997). Therefore, evaluation of SIFs along the crack front in linear elastic fracture mechanics has been considerably investigated. However, accurate calculation of SIFs for three-dimensional (3D) crack surface is still an important computational issue in fracture mechanics.

Irwin first introduced the SIFs to describe the stress and displacement fields near a crack tip in 1957 (Irwin, 1957), and obtained an approximate solution for the crack surface problem in 1962 (Irwin, 1962). Literature associated with this problem is quite extensive and various numerical techniques have been proposed to obtain 3D SIFs in fracture problems. Mi and Aliabadi (1992) presented the 3D dual boundary element method (dual-BEM) for linear elastic crack problems, and used it to overcome the numerical difficulties associated with the two mathematically identical sides of a crack. Singh *et al.* (1998) obtained the SIFs using the concept of a universal crack closure integral in 3D isotropic elastic materials. Pan and Yuan (2000) applied the especial nine-node elements to discretize the un-cracked boundary and the crack surface in an infinite space or a finite cube, and also derived the relation between SIFs and the relative crack opening displacements (CODs) technique. Lazarus *et al.* (2001) compared the mixed-mode I-II or I-II-III SIFs between the theoretical analyses and the experimental results in the brittle solid considering the crack front rotation or segmentation. A new 3D variable-order singular boundary element was presented by Zhou *et al.* (2005). These elements can be used for both straight and curved crack fronts in the embedded penny-shaped homogeneous and bi-material interface crack problems. Leung and Su (1995) used the finite element methods (FEM) to investigate the stress distribution and the variation of the mode-I SIF near the mid-plane of the specimen. He *et al.* (1997) proposed a 3D COD correlation formula to calculate SIFs in 3D fracture problems by using FEM in which the 20-node collapsed iso-parametric quarter-point elements were adopted. Ayatollahi and Hashemi (2007) carried out a 3D finite element analysis to investigate the effect of asymmetric composite reinforcement on the crack tip parameters K_I, K_{II} and T-stress. Yue *et al.* (2007) employed the dual-BEM in their calculation of the 3D SIFs of an inclined square crack within a bi-material cuboid.

In recent years, BEM provides a powerful alternative to FEM particularly in the analysis of 3D fracture problems where better accuracy are required such as damaged material (Hatzigeorgiou and Beskos, 2002); dynamic material (Ariza and Dominguez, 2004); bi-material (Noda *et al.*, 2006; Qin *et al.*, 2008); thermo-elastic material (dell'Erba and Aliabadi, 2000); magneto-electro-elastic material (Zhao *et al.*, 2007); non-linear surface crack (Liu *et al.*, 1999); multiple-crack (Lo *et al.*, 2005; Popov *et al.*, 2003); crack growth (Blackburn, 1999); or where the physical domain extends to infinity (Pan and Yuan, 2000). The most important feature of BEM is that it requires only 2D meshing of the 3D crack surface and the un-crack boundary. BEM is based on the boundary integral equations of displacement and traction, which both being evaluated directly on the boundary. Hence, boundary element codes can be very conveniently used with existing solid modelers and surface mesh generators. This advantage is particularly important for design as the process usually involves a series of modifications, which are more difficult to carry out using FEM. In BEM, the usage of quadrilateral collocation shape functions is a popular method as adopted by many scholars (Ariza *et al.*, 1997; Partheymüller *et al.*, 2000; Ong and Lim, 2005; Mezrhab and Bouzidi, 2005; Guzina *et al.*, 2006).

In this paper, we present the special nine-node quadrilateral collocation shape functions to descretize (or approximate) the surface crack on the partial boundary. A combination of the dual-BEM (or single-domain BEM) and the relative COD is employed to analyze the mixed 3D SIFs in a transversely isotropic cuboid with any oriented isotropic plane and varying crack plane orientation. Numerical results on the edge crack case show that material and crack orientations can significantly influence the mixed SIFs along the front of the edge crack. Our results on the embedded crack case show that when one of the crack fronts moves to the boundary of the cuboid, the corresponding mixed SIFs can be significantly increased.

2. Global and local coordinate system relations

In the present paper, a 3D boundary element analysis is carried out to obtain mode-I, mode-II and mode-III SIFs along the crack front of a rectangular surface crack in a cuboid subjected to a tension loading σ_0 (Figure 1). The orientation between the material and crack are described respectively by the relation between the global (x, y, z) and local material (x', y', z'), and between the global (x, y, z) and local crack (x'', y'', z'') coordinate systems. The surface crack is on the $(x''\text{-}y'')$ plane with its normal being the

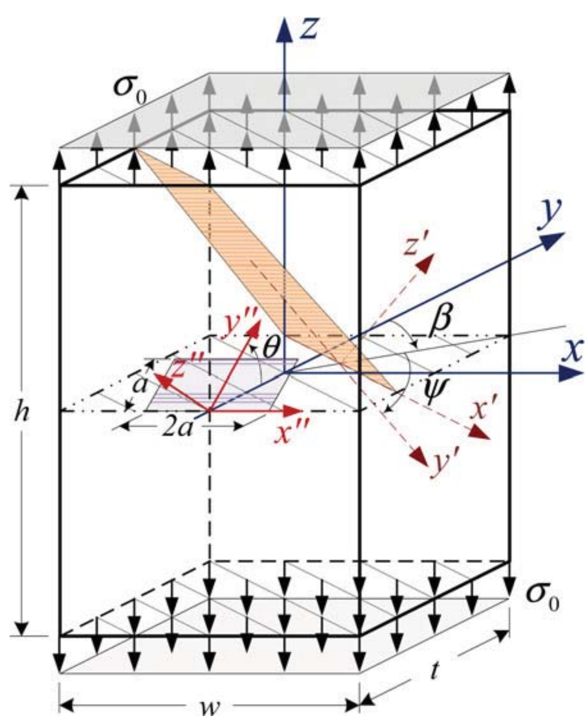

Figure 1.
An edge rectangular crack ($2a \times a$) within a finite cuboid ($w \times t \times h$) under a uniform normal stress σ_0 along the z-direction

z''-axis, and is located inside a transversely isotropic elastic finite domain with arbitrarily oriented transverse isotropy. In the material coordinate, the local z'-axis is along the symmetry axis of the transversely isotropic material, and the local (x'-y') plane is parallel to the isotropic plane of the material. The inclined angle ψ is defined as the angle between the global horizontal plane (x-y) and the material isotropic (x'-y') plane. β is the dip orientation between the y-axis and the inclined plane. In the crack surface, the crack angle θ is defined as the angle between the global horizontal (x-y) plane and the crack surface (x''-y'') plane.

It is obvious that the transformations between the local material (x', y', z') and global (x, y, z) coordinates and between the local crack (x'', y'', z'') and global (x, y, z) can be described by the following relations:

$$\begin{bmatrix} x' \\ y' \\ z' \end{bmatrix} = \begin{bmatrix} \cos\beta & -\sin\beta & 0 \\ \cos\psi\sin\beta & \cos\psi\cos\beta & -\sin\psi \\ \sin\psi\sin\beta & \sin\psi\cos\beta & \cos\psi \end{bmatrix} \begin{bmatrix} x \\ y \\ z \end{bmatrix} \tag{1}$$

$$\begin{bmatrix} x'' \\ y'' + 0.5a \\ z'' \end{bmatrix} = \begin{bmatrix} 1 & 0 & 0 \\ 0 & \cos\theta & \sin\theta \\ 0 & -\sin\theta & \cos\theta \end{bmatrix} \begin{bmatrix} x \\ y + 0.5t \\ z \end{bmatrix} \tag{2}$$

where a is the width of the surface crack along y''-axis; t is the width of the cuboid along y-axis.

3. Boundary integral equations

The displacement and traction boundary integral equations for solving 3D linear elastic fracture problems with cracks are based on the dual-BEM (Aliabadi, 1997) or the single-domain BEM (Pan, 1997) approach. We assume that the finite domain under consideration is bounded by an outer boundary S with given boundary conditions. Inside there is a crack described by its surface Γ (where $\Gamma = \Gamma^+ = -\Gamma^-$, with superscripts "+" and "−" denoting the positive and negative sides of the crack). We further assume that the tractions on both sides of the crack are equal and opposite. Then the single-domain BEM formulation consists of the following displacement and traction boundary integral equations (Pan and Amadei, 1996a):

$$\begin{aligned} c_{ij}(\mathbf{y}_S)u_j(\mathbf{y}_S) &+ \int_S \left[u_j(\mathbf{x}_S)T^*_{ij}(\mathbf{y}_S,\mathbf{x}_S) - t_j(\mathbf{x}_S)U^*_{ij}(\mathbf{y}_S,\mathbf{x}_S)\right] dS(\mathbf{x}_S) \\ &= -\int_\Gamma \left[\Delta u_j(\mathbf{x}_\Gamma)T^*_{ij}(\mathbf{y}_S,\mathbf{x}_{\Gamma^+})\right] d\Gamma(\mathbf{x}_{\Gamma^+}) \end{aligned} \tag{3}$$

$$\begin{aligned} 0.5\Delta T_l(\mathbf{y}_\Gamma) &+ n_m(\mathbf{y}_{\Gamma^+}) \int_S c_{lmik} T^*_{ij,k}(\mathbf{y}_{\Gamma^+},\mathbf{x}_S)u_j(\mathbf{x}_S)dS(\mathbf{x}_S) \\ &+ n_m(\mathbf{y}_{\Gamma^+}) \int_\Gamma \left[\Delta u_j(\mathbf{x}_\Gamma)c_{lmik}T^*_{ij,k}(\mathbf{y}_{\Gamma^+},\mathbf{x}_{\Gamma^+})\right] d\Gamma(\mathbf{x}_{\Gamma^+}) \\ &= n_m(\mathbf{y}_{\Gamma^+}) \int_S c_{lmik}U^*_{ij,k}(\mathbf{y}_{\Gamma^+},\mathbf{x}_S)T_j(\mathbf{x}_S)dS(\mathbf{x}_S) \end{aligned} \tag{4}$$

where c_{ij} are coefficients that depend only upon the local geometry of the uncracked boundary at $\mathbf{y}_S$. A point on the positive (or negative) side of the crack is denoted by $\mathbf{x}_{\Gamma^+}$

(or $\mathbf{x}_{\Gamma^-}$), and on the uncracked boundary by both $\mathbf{x}_S$ and $\mathbf{y}_S$. Also in Equation (3), u_j and t_j represent the displacements and tractions on the boundary (or crack surface), and U^*_{ij} and T^*_{ij}, are the Green's functions for displacements and tractions in general anisotropic elastic solid (Pan and Yuan, 2000). n_m is the unit outward normal of the positive side of the crack surface at $\mathbf{y}_{\Gamma^+}$ and c_{lmik} is the fourth-order stiffness tensor of the anisotropic medium; $U^*_{ij,k}$ and $T^*_{ij,k}$ are, respectively, the derivatives of the Green's displacements and tractions with respect to the source point (Pan and Amadei, 1996b).

The strong singularity of T^*_{ij} on the left-hand side of Equation (3) can be avoided by the rigid-body motion method. At the same time, the calculation of c_{ij} can also be avoided. The second integral term on the left-hand side has only a weak singularity, and is integrable. Equations (3) and (4) form a pair of boundary integral equations, called single-domain BEMs, and they can be applied to generally anisotropic media. They can be discretized and solved numerically for the unknown boundary displacements (or the relative CODs on the crack surface) and tractions. However, before we apply these single-domain BEMs to calculate the mixed SIFs, we first briefly present the special elements and the technique for evaluating the 3D SIF.

4. Discretization of boundary integral equations and SIFs evaluation

In order to solve Equations (3) and (4) numerically, the whole boundary (including the un-cracked boundary and the crack surface) of the cuboid is discretized into nine-node quadrilateral curved elements (Pan and Yuan, 2000). Because of the discontinuities of the displacements across the mouth of the surface crack, the continuous nine-node element need to be modified, as shown in Figure 2. The incompatible new elements are types 3 and 4 shown in Figure 3. Therefore, one requires totally four and six different types of elements, respectively, for the un-cracked boundary and the crack surface, as shown in Figures 3 and 4 to discretize the problem boundary. More specifically, the type 1 element can be used to discretize both regular un-cracked boundary and crack surface. The types 2 and 5 elements are obtained by moving nodes 1-3 with a distance of 1/3 along positive ξ_2-direction; the types 3 and 4 elements are obtained by moving respectively nodes 2 and 3, and 1 and 2 with a distance of 1/3 along positive ξ_2-direction; the types 6 and 8 by moving nodes 1-3 a value of 1/3 along positive ξ_2-direction, and nodes 1, 4 and 7 a value of 1/3 along positive ξ_1-direction. Finally,

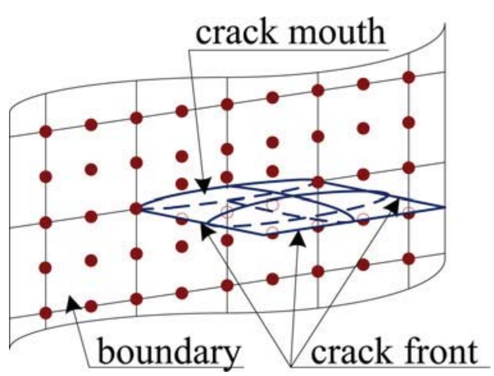

Figure 2.
The boundary mesh at the location where the edge crack joints the outer boundary of the cuboid

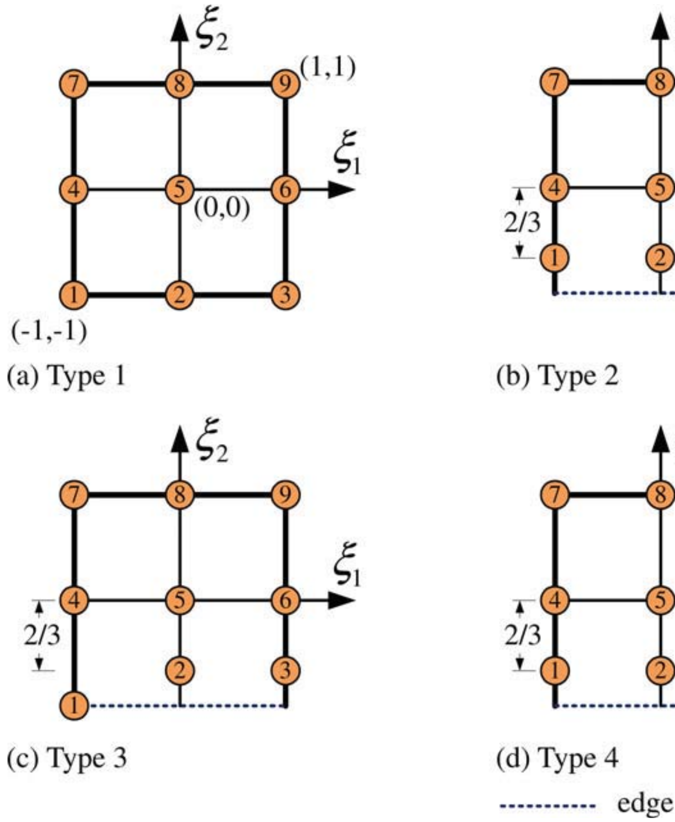

Figure 3. Four different types of elements for un-cracked boundaries

types 7 and 9 are obtained by moving nodes 1-3 a value of 1/3 along positive ξ_2-direction and nodes 3, 6, 9 a value of 1/3 along negative ξ_1-direction.

The global coordinates (x_i), displacements (u_i) and tractions (t_i) at any point within one element on the un-cracked boundary can be expressed as:

$$x_i(\xi) = \sum_{j=1}^{9} \phi_j(\xi) x_i^j, \quad u_i(\xi) = \sum_{j=1}^{9} \phi_j(\xi)\, u_i^j, \quad t_i(\xi) = \sum_{j=1}^{9} \phi_j(\xi)\, t_i^j, \quad i = 1,2,3 \tag{5}$$

where the subscript i denotes the component of nodal coordinates and the superscript j denotes the number of nodes. The shape functions ϕ_j (j = 1-9) are functions of the intrinsic coordinates (ξ_1, ξ_2), and their expressions for different elements are listed in the Appendix.

Similarly, the relative CODs Δu_i ($\Delta u_i = u_i^{\Gamma+} - u_i^{\Gamma-}$) on the crack surface can be approximated as:

$$\Delta u_i = \sum_{j=1}^{9} \phi_j\, \Delta u_i^j, \quad i = 1,2,3 \tag{6}$$

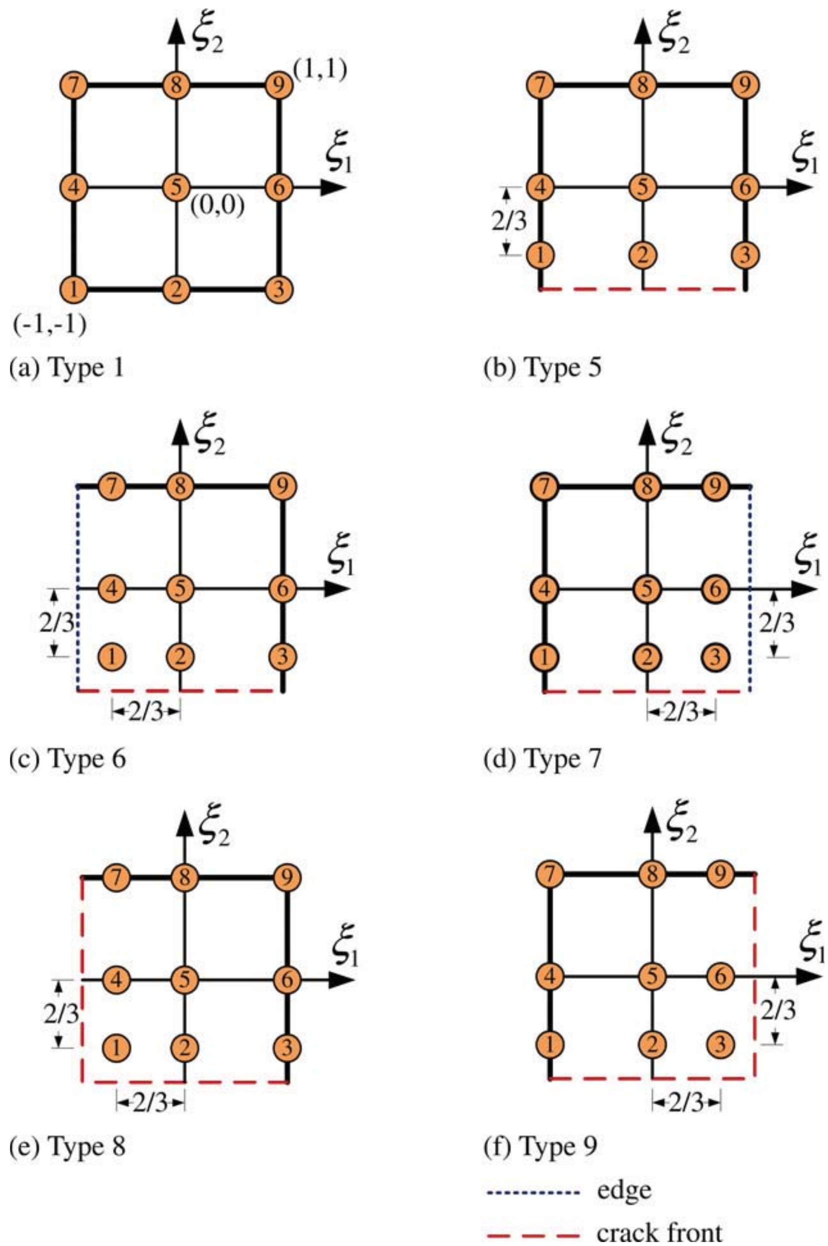

Figure 4.
Six different types of elements for the crack surface

However, for the relative CODs on the crack element near a crack front, the crack shape functions are multiplied by suitable weight functions for accurate evaluation of the SIFs. It is well-known that for a crack in a homogeneous and anisotropic solid, the relative CODs are proportional to $\sqrt{r}$, where r is the distance behind the crack tip (front). Therefore, for element types 5-7 (Figure 4), we employ the following approximation for the relative CODs:

$$\Delta u_i = \sum_{j=1}^{9} \sqrt{(1+\xi_2)}\phi_j \Delta u_i^j, \quad i = 1,2,3 \tag{7}$$

where ϕ_j are again the shape functions given in the Appendix.

In addition, we use the following two approximations for element types 8 and 9, respectively:

$$\Delta u_i = \sum_{j=1}^{9} \sqrt{(1+\xi_1)(1+\xi_2)}\phi_j \Delta u_i^j, \quad i = 1,2,3 \tag{8}$$

$$\Delta u_i = \sum_{j=1}^{9} \sqrt{(1-\xi_1)(1+\xi_2)}\phi_j \Delta u_i^j, \quad i = 1,2,3 \tag{9}$$

Once the relative CODs are solved in the global coordinates, they can be transformed to the local coordinates (or the crack tip coordinates) to find the SIFs. Assuming that the crack front is smooth and that the crack tip is away from the corner, then the asymptotic expansion of the relative COD field near the crack tip (front) satisfies the generalized plane strain condition in the local coordinates. Actually, if we let r be the distance behind the crack front, then in terms of the relative CODs in the crack-tip coordinate, the three SIFs can be expressed as follows:

$$\begin{Bmatrix} K_{II} \\ K_I \\ K_{III} \end{Bmatrix} = 2\sqrt{\frac{2r}{\pi}}\mathbf{L}^{-1} \begin{Bmatrix} \Delta u_1 \\ \Delta u_2 \\ \Delta u_3 \end{Bmatrix} \tag{10}$$

where $\mathbf{L}$ is the Barnett-Lothe tensors (Ting, 1996) which depends only on the anisotropic properties of the solid in the crack front coordinates. The normalized SIFs (F_I, F_{II} and F_{III}) can be calculated as follows:

$$\begin{Bmatrix} F_I \\ F_{II} \\ F_{III} \end{Bmatrix} = \sigma_0^{-1}\sqrt{\frac{1}{\pi a}} \begin{Bmatrix} K_I \\ K_{II} \\ K_{III} \end{Bmatrix} \tag{11}$$

where σ_0 is the applied vertical traction in the problem to be discussed below.

5. Numerical results and discussion

Consider a linearly elastic, homogeneous, and transversely isotropic cuboid with dimension $w \times t \times h$, as shown in Figure 1. Let x, y and z be the global Cartesian coordinates with their origin in the center of the cuboid. A rectangular surface crack of $2a \times a$ is located in the cuboid with one of its sides along the edge of the cuboid. A local coordinate system (x'', y'', z'') is attached to the crack with its z''-axis normal to the crack surface. The angle of crack orientation θ is defined as the angle between the global horizontal (x-y) plane and the crack (x''-y'') plane.

The cracked finite cuboid is under a uniform normal tensile stress σ_0 applied at the top and bottom faces, as shown in Figure 1. In the numerical example, the cuboid size is chosen to be $w/t = 2$, $h/t = 4$ and the size of rectangular crack $2a/t = 1$. The material of the cuboid is a transversely isotropic marble and its elastic properties were obtained experimentally (Chen *et al.*, 2008) as $E = 90$ GPa, $E' = 55$ GPa, $\nu = \nu' = 0.3$, $G = 35$ GPa and $G' = 21$ GPa. After checking our program for a couple of special cases for accuracy, 64 and 32 nine-nodal quadrilateral elements are used to discretize the un-cracked boundary and the cracked surface, respectively, for the numerical examples presented below. Furthermore, the SIFs are plotted along the crack fronts (i.e. AB, BC and CD), as shown in Figure 5.

The variation of the normalized mode-I SIF (F_I) along the crack front for different inclined angles of the material with fixed angle $\beta = 0°$ are shown in Figure 6. For a horizontal crack ($\theta = 0°$), six types of materials, i.e. the transversely isotropic rocks with six different inclined angles $\psi = 0°$, 15°, 30°, 45°, 60° and 75°, were selected to calculate the variation of the mode-I, mode-II and mode-III SIFs along the crack fronts. It is observed that the maximum value of F_I is equal to 1.33 and occurred in the middle of the crack front BC for the material inclined angle $\psi = 60°$. However, along the crack fronts AB and CD, the maximum value of F_I is reached when $\psi = 45°$. It is also noted

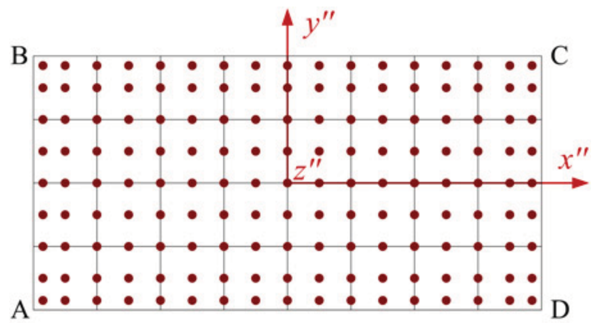

Notes: For the edge crack case, AB, BC and CD are the crack fronts and AD is the crack edge. For the embedded crack case, the four sides are all the crack fronts

Figure 5.
Discretization of the rectangular crack by 32 nine-node quadrilateral elements

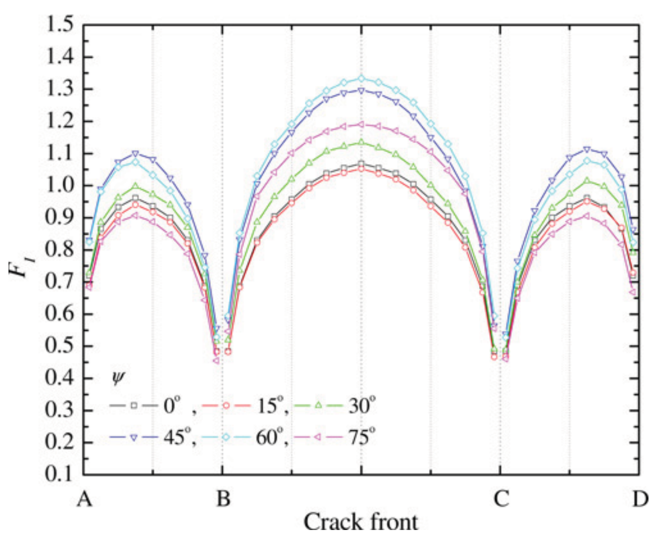

Figure 6.
The normalized mode-I SIF along the horizontal ($\theta = 0°$) rectangular crack fronts AB, BC and CD for six different material inclined angle ψ with fixed $\beta = 0°$ within a finite transversely isotropic cuboid

that the SIF F_I is symmetric along the crack fronts AB and CD only when $\psi = 0°$. It is also interesting that since the material dip angle $\beta = 0°$ and crack angle $\theta = 0°$, the SIF F_I is symmetric with respect to the middle point of the crack front BC, and that the SIF F_I along AB is the same as that along DC. Furthermore, the magnitude of F_I along BC is, in general, larger than that along AB or CD for a given material angle ψ.

Figures 7 and 8 show, respectively, the variation of the normalized mode-II SIF (F_{II}) and mode-III (F_{III}) along the crack fronts AB, BC and CD for different material angle ψ ($\beta = 0°$) with fixed angle orientation ($\theta = 0°$). Compared to Figure 6, we observed that the magnitude of the SIF for mode II and III is much smaller than that for mode-I. We also noted from Figures 7 and 8 that the SIF value for mode II and III can be both

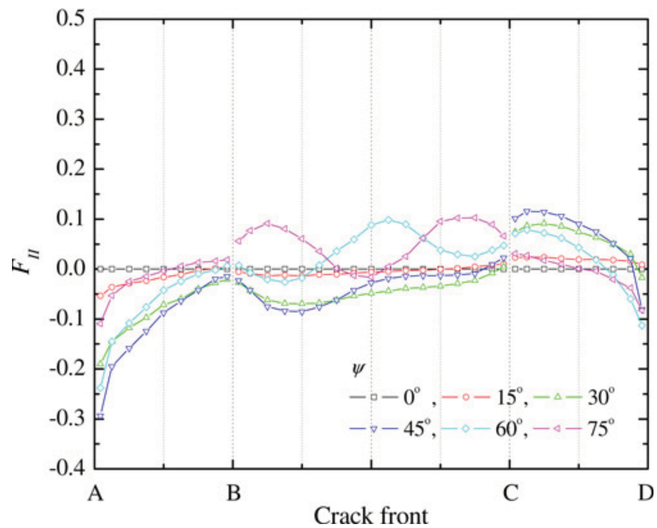

Figure 7.
The normalized mode-II SIF along the horizontal ($\theta = 0°$) rectangular crack fronts AB, BC and CD for six different material inclined angle ψ with fixed $\beta = 0°$ within a finite transversely isotropic cuboid

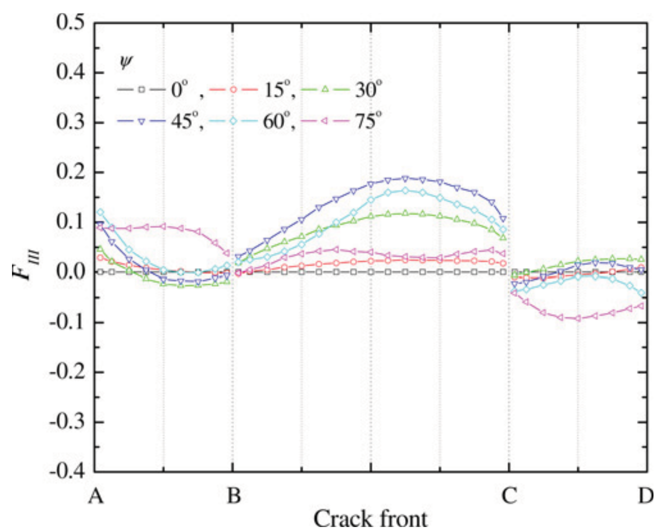

Figure 8.
The normalized mode-III SIF along the horizontal ($\theta = 0°$) rectangular crack fronts AB, BC and CD for six different material inclined angle ψ with fixed $\beta = 0°$ within a finite transversely isotropic cuboid

positive and negative, indicating that the crack shearing and tearing can occur in different directions for different material orientations or along different crack fronts.

The variation of the SIFs along the crack front for different orientations of material and crack are shown in Figures 9-11, where the material orientation angles (ψ, β) are both (0°, 0°) and (60°, 30°), and crack angles (θ) are 15°, 30° and 45°. Figure 9 shows the variation of the normalized mode-I SIF F_I. It is observed that along BC the curve is symmetric when $\psi = 0°$ and $\beta = 0°$, and that the maximum value for the crack angle $\theta = 15°$ is larger than that for $\theta = 45°$ (0.958 vs 0.45 in Figure 9). Furthermore, the magnitude of SIF F_I increases with decreasing crack angle. For the material angle (60°, 30°), the magnitude of the maximum in F_I is roughly 6.25 percent larger than its

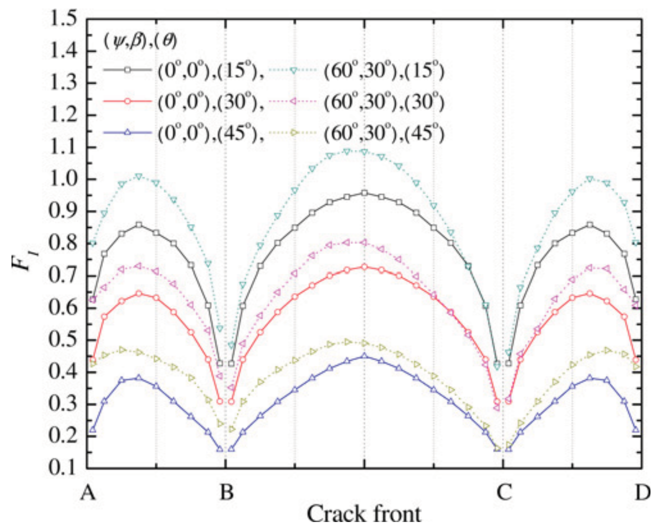

Figure 9.
The normalized mode-I SIF along the rectangular crack fronts AB, BC and CD for two different material orientations (0°, 0°) and (60°, 30°), and three different crack orientations (15°, 30° and 45°) within a finite transversely isotropic cuboid

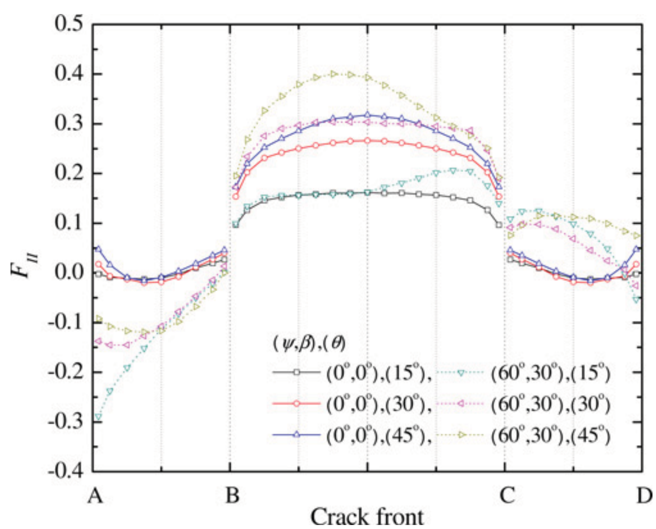

Figure 10.
The normalized mode-II SIF along the rectangular crack fronts AB, BC and CD for two different material orientations (0°, 0°) and (60°, 30°), and three different crack orientations (15°, 30° and 45°) within a finite transversely isotropic cuboid

value at the center of BC, due to the effects of inclined angle and dip angle. The maximum value for the crack angle $\theta = 15°$ is larger than that $\theta = 45°$ (1.09 vs 0.49 in Figure 9). It is noted that the magnitude of F_I along AB and CD is roughly the same as that along BC. As for the mode-II and mode-III, we observed from Figures 10 and 11 that the SIF variation for the shearing and tearing modes F_{II} and F_{III} is much complicated than that of F_I. Similar to Figures 7 and 8 for $\beta = 0°$ and $\theta = 0°$, shearing and tearing in different directions can be observed along different crack fronts.

We study the effect of the crack distance (to the free edge of the cuboid) on the SIFs. Different distance ratios d/t (=0, 0.05, 0.1, 0.15, 0.2 and 0.25) are selected, whilst the crack size is kept constant, as shown in Figure 12. The material angles are also fixed at $\psi = \beta = 0°$. The results of the mode-I SIF F_{I} for the edge crack (i.e. $d/t = 0$) as well as the embedded crack (i.e. $d/t = 0.05$, 0.1, 0.15, 0.2 and 0.25) are plotted in Figure 13. It is noted that when $d/t = 0$ the crack front DA becomes the crack mouth. Our numerical results show that the F_I value increases with decreasing distance d/t, and that the results along the crack front AB are the same as that along CD due to the symmetry of the problem. It is interesting to observe that the maximum SIF along DA is larger than that along BC (1.17 vs 1.07). This phenomenon is due to the fact that the crack front

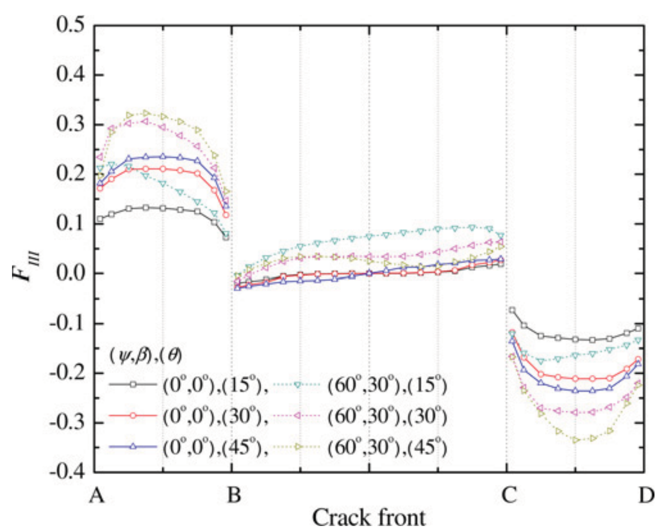

Figure 11.
The normalized mode-III SIF along the rectangular crack fronts AB, BC and CD for two different material orientations (0°, 0°) and (60°, 30°), and three different crack orientations (15°, 30° and 45°) within a finite transversely isotropic cuboid

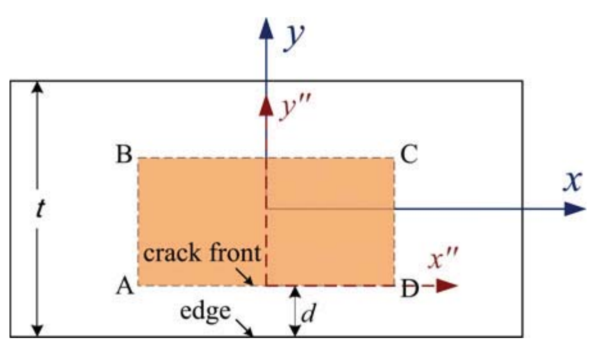

Figure 12.
An embedded horizontal rectangular crack located on the $z = 0$ plane of a finite cuboid. The crack front AD intercepts the outer boundary of the cuboid when the crack moves to the surface along the negative y-direction

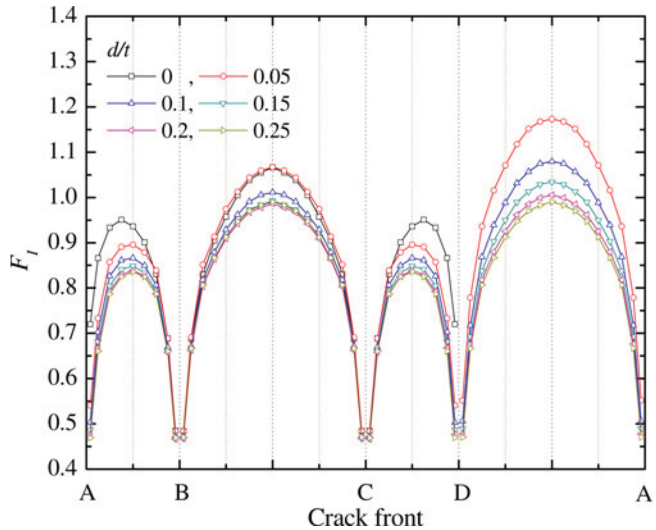

Figure 13.
Normalized mode-I SIF along the crack fronts AB, BC, CD and DA for different crack distance (to the boundary of the cuboid) *d/t* from 0 to 0.25

along DA is closer to the edge of cuboid than the front BC. When the crack is located in the center of cuboid ($d/t = 0.25$), the SIF variation becomes the same along the crack fronts BC and DA. The maximum SIF values along different crack fronts for different distance *d/t* are presented in Table I in order to show quantitatively those the effect of the crack distance on the SIFs.

Finally, we also study the interactive effect of two edged cracks on SIFs, as shown in Figure 14. The relative distance ratio *L/t* (=0.3, 0.5 and 0.7) are selected to discuss the variation of the normalized mode-I, mode-II and mode-III SIFs along the crack front BC. For two horizontal cracks ($\theta = 0°$), the results of the normalized SIFs with the seven different material inclined angle $\psi = 0°$ to $90°$ (β is fixed at 30°) are plotted in Figure 15. It is observed that the maximum value of F_I is equal to 1.64 and occurred in the $L/t = 0.3$ for the material inclined angle $\psi = 45°$. However, the magnitude of SIF FI decreases with increasing distance ratio *L/t*. It is noted that the interactive effect of two edged rectangular cracks is changed with respect to both the distance ratio and material angle. For the mode-II and mode-III SIFs, we observed from Figure 15 that the magnitudes of F_I and F_{II} along crack front BC are large variation when $\psi = 45°$. When the material angle is fixed at $\psi = \beta = 0°$, the maximum normalized mode-I SIF values along the crack fronts AB, BC and CD are presented in Table II. The result shows that the values of SIF FI decreases with increasing distance ratio *L/t* (0.3 to 0.8) in order to signify the interactive effect of the relative crack distance on the SIFs.

Table I.
Maximum normalized mode-I SIF along the crack fronts AB, BC, CD and DA of the rectangular crack for different crack distance (to the outer boundary of the cuboid) *d/t*

	Crack front			
d/t	AB	BC	CD	DA
0	0.951	1.066	0.951	–
0.05	0.896	1.067	0.896	1.173
0.1	0.866	1.011	0.866	1.080
0.15	0.849	0.993	0.849	1.034
0.2	0.839	0.986	0.839	1.005
0.25	0.836	0.990	0.836	0.990

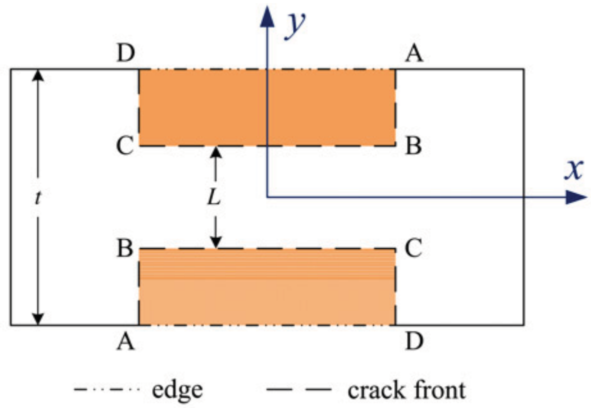

Notes: The distance L changed when the two crack sizes vary along the y-direction

Figure 14. Two edged horizontal rectangular cracks located on the $z = 0$ plane of a finite cuboid

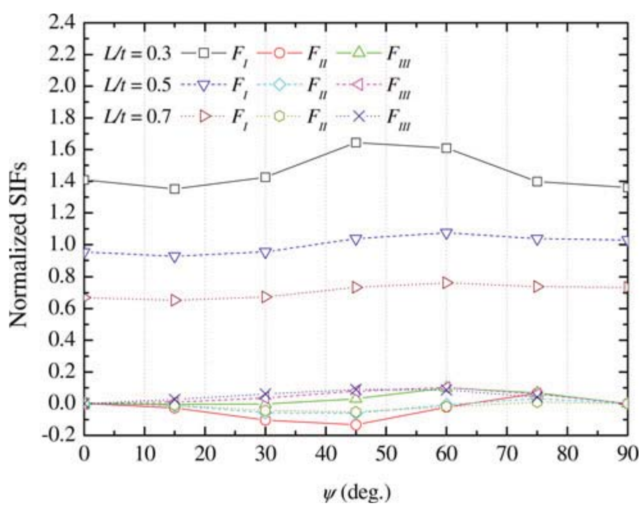

Figure 15. Normalized SIFs on $x = 0$ along the crack front BC for three different crack interactive distances L/t and seven different material inclined angle ψ with fixed $\beta = 30°$ within a finite transversely isotropic cuboid

	Crack front		
L/t	AB	BC	CD
0.3	1.193	1.408	1.193
0.4	0.988	1.120	0.988
0.5	0.862	0.959	0.862
0.6	0.745	0.831	0.745
0.7	0.617	0.697	0.617
0.8	0.477	0.574	0.477

Table II. Maximum normalized mode-I SIF along the crack fronts AB, BC and CD of two edged rectangular cracks for different relative distance L/t

6. Conclusions

In this study, the normalized mode-I, mode-II and mode-III SIFs along the crack front of a rectangular crack in a cuboid are calculated based on the dual-BEM or the single-domain BEM. Both the crack orientation and material orientation (including the inclined angle and dip angle) of the transversely isotropic cuboid can be varied. A set of six special nine-node quadrilateral elements are introduced to approximate the crack front and the mixed 3D SIFs are evaluated using the asymptotical relation between the SIFs and the relative COD via the Barnett-Lothe tensor. Numerical examples of the mixed 3D SIFs are presented for the transversely isotropic cracked cuboid under a uniform vertical traction on its top and bottom surfaces. Results show that for a horizontal edge crack, the mode-I is symmetric with respect to the middle of the crack front when the material inclined angle $\psi = 0°$ ($\theta = 0°$); otherwise the SIF values are asymmetric. Variations of the SIFs for mode-II and mode-III along the crack fronts are complicated with shearing and tearing in different directions being observed. For an embedded rectangular crack, it is observed that when the crack moves away from the edge, the mode-I SIF will be reduced. For two edged rectangular cracks, the interactive effect on SIFs is varied with both the material orientation and relative crack distance.

References

Aliabadi, M.H. (1997), "Boundary element formulations in fracture mechanics", *Applied Mechanics Review*, Vol. 50, pp. 83-96.

Ariza, M.P. and Dominguez, J. (2004), "Dynamic BE analysis of 3-D cracks in transversely isotropic solids", *Computer Methods in Applied Mechanics and Engineering*, Vol. 193, pp. 765-79.

Ariza, M.P., Saez, A. and Dominguez, J. (1997), "A singular element for three-dimensional fracture mechanics analysis", *Engineering Analysis with Boundary Elements*, Vol. 20, pp. 275-85.

Ayatollahi, M.R. and Hashemi, R. (2007), "Computation of stress intensity factors (K_{I}, K_{II}) and T-stress for cracks reinforced by composite patching", *Composite Structure*, Vol. 78, pp. 602-9.

Blackburn, W.S. (1999), "Three dimensional calculation of growth of cracks starting in parallel planes by boundary elements", *Internal Journal of Fatigue*, Vol. 21, pp. 933-9.

Chen, C.H., Chen, C.S. and Wu, J.H. (2008), "Fracture toughness analysis on cracked ring disks of anisotropic rock", *Rock Mechanics and Rock Engineering.*, Vol. 41 No. 4, pp. 539-62.

dell'Erba, D.N. and Aliabadi, M.H. (2000), "On the solution of three-dimensional thermoelastic mixed-mode edge crack problems by the dual boundary element method", *Engineering. Fracture Mechanics*, Vol. 66, pp. 269-85.

Guzina, B.B., Pak, R.Y.S. and Martínez-Castro, A.E. (2006), "Singular boundary elements for three-dimensional elasticity problems", *Engineering Analysiswith Boundary Elements*, Vol. 30, pp. 623-39.

Hatzigeorgiou, G.D. and Beskos, D.E. (2002), "Static analysis of 3D damaged solids and structures by BEM", *Engineering Analysis with Boundary Elements*, Vol. 26, pp. 521-6.

He, W.J., Lin, Y. and Ding, H.J. (1997), "A three-dimensional formula for determining stress intensity factors in finite element analysis of cracked bodies", *Engineering Fracture Mechanics*, Vol. 57 No. 4, pp. 409-15.

Irwin, G.R. (1957), "Analysis of stresses and strains near the end of a crack traversing a plate", *Journal of Applied. Mechanics*, Vol. 24, pp. 361-4.

Irwin, G.R. (1962), "Crack extension force for a part-through crack in a plate", *Journal of Applied Mechanics, Transactions ASME*, Vol. 29 No. 4, pp. 651-4.

Lazarus, V., Leblond, J.B. and Mouchrif, S.E. (2001), "Crack front rotation and segmentation in mixed mode I + III or I + II + III. Part I: calculation of stress intensity factors", *Journal of the Mechanics and Physics of Solids*, Vol. 49, pp. 1399-420.

Leung, A.Y.T. and Su, R.K.L. (1995), "A numerical study of singular stress field of 3D cracks", *Finite Elements in Analysis and Design*, Vol. 18, pp. 389-401.

Liu, Y., Liang, L.H., Hong, Q.C. and Antes, H. (1999), "Non-linear surface crack analysis by three dimensional boundary element with mixed boundary conditions", *Engineering Fracture Mechanics*, Vol. 63, pp. 413-24.

Lo, S.H., Dong, C.Y. and Cheung, Y.K. (2005), "Integral equation approach for 3D multiple-crack problems", *Engineering Fracture Mechanics*, Vol. 72, pp. 1830-40.

Mezrhab, A. and Bouzidi, M. (2005), "Computation of view factors for surfaces of complex shape including screening effects and using a boundary element approximation", *Engineering and Computations*, Vol. 22 No. 2, pp. 132-48.

Mi, Y. and Aliabadi, M.H. (1992), "Dual boundary element method for three-dimensional fracture mechanics analysis", *Engineering Analysis with Boundary Elements*, Vol. 10 No. 2, pp. 161-71.

Noda, N.A., Kouyama, T. and Kinoshita, Y. (2006), "Stress intensity factors of an inclined elliptical crack near a biomaterial interface", *Engineering Fracture Mechanics*, Vol. 73, pp. 1292-320.

Ong, E.T. and Lim, K.M. (2005), "Three-dimensional singular boundary elements for corner and edge singularities in potential problems", *Engineering Analysis with Boundary Elements*, Vol. 29, pp. 175-89.

Pan, E. (1997), "A general boundary element analysis of 2-D linear elastic fracture mechanics", *International Journal of Fracture*, Vol. 88, pp. 41-59.

Pan, E. and Amadei, B. (1996a), "Fracture mechanics analysis of cracked 2-D anisotropic media with a new formulation of the boundary element method", *International Journal of Fracture*, Vol. 77, pp. 161-74.

Pan, E. and Amadei, B. (1996b), "A 3-D boundary element formulation of anisotropic elasticity with gravity", *Applied Mathematical Modelling*, Vol. 20, pp. 114-20.

Pan, E. and Yuan, F.G. (2000), "Boundary element analysis of three-dimensional cracks in anisotropic solids", *International Journal for Numerical Methods in Engineering*, Vol. 48 pp. 211-37.

Partheymüller, P., Haas, M. and Kuhn, G. (2000), "Comparison of the basic and the discontinuity formulation of the 3D-dual boundary element method", *Engineering Analysis with Boundary Elements*, Vol. 24, pp. 777-88.

Popov, V., Power, H. and Walker, S.P. (2003), "Numerical comparison between two possible multipole alternatives for the BEM solution of 3D elasticity problems based upon Taylor series expansions", *Engineering Analysis with Boundary Elements*, Vol. 27, pp. 521-31.

Qin, T.Y., Zhu, B.J. and Noda, N.A. (2008), "Mixed-mode stress intensity factors of a three-dimensional crack in a bonded biomaterial", *Engineering Computations*, Vol. 25 No. 3, pp. 251-67.

Singh, R., Carter, B.J., Wawrzynek, P.A. and Ingraffea, A.R. (1998), "Universal crack closure integral for SIF estimation", *Engineering Fracture Mechanics*, Vol. 60 No. 2, pp. 133-46.

Ting, T.C.T. (1996), *Anisotropic Elasticity: Theory and Applications*, Oxford University Press, New York, NY.

Toribio, J. and Kharin, V. (1997), "The reliability of the fracture mechanics approach to environmentally assisted cracking: 2. Engineering safe design", *Materials and Design*, Vol. 18 No. 2, pp. 95-101.

Yue, Z.Q., Xiao, H.T. and Pan, E. (2007), "Stress intensity factors of square crack inclined to interface of transversely isotropic bi-material", *Engineering Analysis with Boundary Elements*, Vol. 31, pp. 50-65.

Zhao, M.H., Fan, C.Y., Liu, T. and Yang, F. (2007), "Extended displacement discontinuity Green's functions for three-dimensional transversely isotropic magneto-electro-elastic media and applications", *Engineering Analysis with Boundary Elements*, Vol. 31, pp. 547-58.

Zhou, W., Lim, K.M., Lee, K.H. and Tay, A.A.O. (2005), "A new variable-order singular boundary element for calculating stress intensity factors in three-dimensional elasticity problems", *International Journal of Solids and Structures*, Vol. 42, pp. 159-85.

Appendix: six shape functions for the nine special element types

I. Shape functions for element type 1

$$\begin{aligned}
\phi_1 &= 0.25\xi_1\xi_2(\xi_1 - 1)(\xi_2 - 1)\\
\phi_2 &= 0.5\xi_2(1 - \xi_1^2)(\xi_2 - 1)\\
\phi_3 &= 0.25\xi_1\xi_2(\xi_1 + 1)(\xi_2 - 1)\\
\phi_4 &= 0.5\xi_1(\xi_1 - 1)(1 - \xi_2^2)\\
\phi_5 &= (1 - \xi_1^2)(1 - \xi_2^2)\\
\phi_6 &= 0.5\xi_1(\xi_1 + 1)(1 - \xi_2^2)\\
\phi_7 &= 0.25\xi_1\xi_2(\xi_1 - 1)(\xi_2 + 1)\\
\phi_8 &= 0.5\xi_2(1 - \xi_1^2)(\xi_2 + 1)\\
\phi_9 &= 0.25\xi_1\xi_2(\xi_1 + 1)(\xi_2 + 1)
\end{aligned} \tag{A1}$$

II. Shape functions for element types 2 and 5

$$\begin{aligned}
\phi_1 &= 0.45\xi_1\xi_2(\xi_1 - 1)(\xi_2 - 1)\\
\phi_2 &= 0.9\xi_2(1 - \xi_1^2)(\xi_2 - 1)\\
\phi_3 &= 0.45\xi_1\xi_2(\xi_1 + 1)(\xi_2 - 1)\\
\phi_4 &= 0.75\xi_1(\xi_1 - 1)(1 - \xi_2)(\xi_2 + 2/3)\\
\phi_5 &= 1.5(\xi_1^2 - 1)(\xi_2 - 1)(\xi_2 + 2/3)\\
\phi_6 &= 0.75\xi_1(\xi_1 + 1)(1 - \xi_2)(\xi_2 + 2/3)\\
\phi_7 &= 0.3\xi_1\xi_2(\xi_1 - 1)(\xi_2 + 2/3)\\
\phi_8 &= 0.6\xi_2(1 - \xi_1^2)(\xi_2 + 2/3)\\
\phi_9 &= 0.3\xi_1\xi_2(\xi_1 + 1)(\xi_2 + 2/3)
\end{aligned} \tag{A2}$$

III. Shape functions for element types 6 and 8

$$\begin{aligned}
\phi_1 &= 0.81\xi_1\xi_2(\xi_1 - 1)(\xi_2 - 1)\\
\phi_2 &= 1.35\xi_2(1 - \xi_1)(\xi_1 + 2/3)(\xi_2 - 1)\\
\phi_3 &= 0.54\xi_1\xi_2(\xi_1 + 2/3)(\xi_2 - 1)\\
\phi_4 &= 1.35\xi_1(\xi_1 - 1)(1 - \xi_2)(\xi_2 + 2/3)\\
\phi_5 &= 2.25(1 - \xi_1)(\xi_1 + 2/3)(1 - \xi_2)(\xi_2 + 2/3)\\
\phi_6 &= 0.9\xi_1(\xi_1 + 2/3)(1 - \xi_2)(\xi_2 + 2/3)\\
\phi_7 &= 0.54\xi_1\xi_2(\xi_1 - 1)(\xi_2 + 2/3)\\
\phi_8 &= 0.9\xi_2(1 - \xi_1)(\xi_1 + 2/3)(\xi_2 + 2/3)\\
\phi_9 &= 0.36\xi_1\xi_2(\xi_1 + 2/3)(\xi_2 + 2/3)
\end{aligned} \tag{A3}$$

IV. Shape functions for element types 7 and 9

$$\begin{aligned}
\phi_1 &= 0.54\xi_1\xi_2(\xi_1 - 2/3)(\xi_2 - 1)\\
\phi_2 &= -1.35\xi_2(1 - \xi_1)(\xi_1 - 2/3)(\xi_2 - 1)\\
\phi_3 &= 0.81\xi_1\xi_2(\xi_1 + 1)(\xi_2 - 1)\\
\phi_4 &= 0.9\xi_1(\xi_1 - 2/3)(1 - \xi_2)(\xi_2 + 2/3)\\
\phi_5 &= -2.25(1 + \xi_1)(\xi_1 - 2/3)(1 - \xi_2)(\xi_2 + 2/3)\\
\phi_6 &= 1.35\xi_1(\xi_1 + 1)(1 - \xi_2)(\xi_2 + 2/3)\\
\phi_7 &= 0.36\xi_1\xi_2(\xi_1 - 2/3)(\xi_2 + 2/3)\\
\phi_8 &= -0.9\xi_2(1 + \xi_1)(\xi_1 - 2/3)(\xi_2 + 2/3)\\
\phi_9 &= 0.54\xi_1\xi_2(\xi_1 + 1)(\xi_2 + 2/3)
\end{aligned} \tag{A4}$$

V. Shape functions for element type 3

$$\begin{aligned}
\phi_1 &= 0.25\xi_1\xi_2(\xi_1 - 1)(\xi_2 - 1)\\
\phi_2 &= 0.9\xi_2(1 - \xi_1^2)(\xi_2 - 1)\\
\phi_3 &= 0.45\xi_1\xi_2(\xi_1 + 1)(\xi_2 - 1)\\
\phi_4 &= 0.5\xi_1(\xi_1 - 1)(1 - \xi_2^2)\\
\phi_5 &= 1.5(\xi_1^2 - 1)(\xi_2 - 1)(\xi_2 + 2/3)\\
\phi_6 &= 0.75\xi_1(\xi_1 + 1)(1 - \xi_2)(\xi_2 + 2/3)\\
\phi_7 &= 0.25\xi_1\xi_2(\xi_1 - 1)(\xi_2 + 1)\\
\phi_8 &= 0.6\xi_2(1 - \xi_1^2)(\xi_2 + 2/3)\\
\phi_9 &= 0.3\xi_1\xi_2(\xi_1 + 1)(\xi_2 + 2/3)
\end{aligned} \tag{A5}$$

VI. Shape functions for element type 4

$$\begin{aligned}
\phi_1 &= 0.45\xi_1\xi_2(\xi_1 - 1)(\xi_2 - 1)\\
\phi_2 &= 0.9\xi_2(1 - \xi_1^2)(\xi_2 - 1)\\
\phi_3 &= 0.25\xi_1\xi_2(\xi_1 + 1)(\xi_2 - 1)\\
\phi_4 &= 0.75\xi_1(\xi_1 - 1)(1 - \xi_2)(\xi_2 + 2/3)\\
\phi_5 &= 1.5(\xi_1^2 - 1)(\xi_2 - 1)(\xi_2 + 2/3)\\
\phi_6 &= 0.5\xi_1(\xi_1 + 1)(1 - \xi_2^2)\\
\phi_7 &= 0.3\xi_1\xi_2(\xi_1 - 1)(\xi_2 + 2/3)\\
\phi_8 &= 0.6\xi_2(1 - \xi_1^2)(\xi_2 + 2/3)\\
\phi_9 &= 0.25\xi_1\xi_2(\xi_1 + 1)(\xi_2 + 1)
\end{aligned} \tag{A6}$$

Corresponding author
Chao-Shi Chen can be contacted at: chencs@mail.ncku.edu.tw